Diffusion Limitations in the Porous Anodes of SOFCs

Journal of The Electrochemical Society, **150** (8) A1067-A1072 (2003)
0013-4651/2003/150(8)/A1067/6/$7.00 © The Electrochemical Society, Inc.

Diffusion Limitations in the Porous Anodes of SOFCs

R. E. Williford,*,z L. A. Chick, G. D. Maupin,* S. P. Simner, and J. W. Stevenson*

Pacific Northwest National Laboratory, Richland, Washington 99352, USA

Concentration polarization is important because it determines the maximum power output of a solid oxide fuel cell (SOFC) at high fuel utilization. Anodic concentration polarization occurs when the demand for reactants exceeds the capacity of the porous cermet anode to supply them by gas diffusion mechanisms. High tortuosities (bulk diffusion resistances) are often assumed to explain this behavior. However, recent experiments show that anodic concentration polarization originates in the immediate vicinity of the reactive triple phase boundary (TPB) sites near the anode/electrolyte interface. A model is proposed to describe how concentration polarization is controlled by two localized phenomena: competetive adsorption of reactants in areas adjacent to the reactive TPB sites, followed by relatively slow surface diffusion to the reactive sites. Results suggest that future SOFC anode design improvements should focus on optimization of the reactive area, adsorption, and surface diffusion at the anode/electrolyte interface.
 [DOI: 10.1149/1.1586300]

Manuscript submitted August 14, 2002; revised manuscript received February 11, 2003. Available electronically June 16, 2003.

It is generally agreed[1] that the hydrogen-oxygen reaction in solid oxide fuel cells (SOFCs) actually occurs in a limited region inside the anode, in an approximately 10 μm thick layer adjacent to the anode/electrolyte interface (the ''reactive zone'' in Fig. 1). The reason for the spatial limitation is that although the hydrogen is supplied by gaseous diffusion through the anode pores, the oxygen is supplied by a solid state vacancy transport mechanism through the electrolyte and the yttria-stabilized-zirconia (YSZ) phase of the anode. Kinetically, the demand for free energy reduction by chemical reaction at anode/electrolyte interface depletes the oxygen before it can diffuse very far into the anode. From a materials science perspective, the finite ionic conductivity of YSZ limits the spatial extent of the oxygen vacancy transport. Within the anode reactive zone, the reaction actually occurs at the triple phase boundaries (TPBs) between the gaseous fuel, the Ni catalyst particles, and the YSZ solid-state oxygen conductor.

The performance of an SOFC is often described by its voltage-current (I-V) relationship, as shown in Fig. 2. At low and midrange currents in modern SOFCs, the response is dominated by the transfer of electrons across the material interfaces, and is often described by the well-known Butler-Volmer equation.[2,3] The high current region is dominated by a precipitous drop in the voltage (and power output) at a limiting, or maximum, current capacity. This ''concentration polarization'' is caused primarily by diffusion limitations in the porous anode, and is the subject of this paper. Because similar limitations can occur in other porous electrode designs, the basic concepts and models presented herein could conceivably be applied to those cases as well.

Many modern SOFC simulation models do not adequately predict the onset of the limiting current described above. This is important because it determines the performance envelope of the device, when fuel utilization approaches 100%, and thus sets goals for device improvements. A primary symptom of model deficiencies is the need to invoke anode tortuosities in the range of 10 to 17.[2-4] The tortuosity, τ, determines the rate of diffusional transport through the porous material via the effective diffusion coefficients $D_i^{eff} = D_i\phi/\tau$, where D_i is the gas phase diffusion coefficient for species i and ϕ is the porosity. Such high tortuosities do not seem reasonable when the observed range for porous sintered ceramics is usually 2-10, and most often in the range of 2-6.[5] Although high apparent tortuosities can be derived based on Fickean diffusional analyses, they are in fact simple empiricisms, and are often unreliable.[6] A more detailed analysis employing Maxwell-Stefan diffusional concepts can lead to different results.[7] Results depend on the definition of the diffusion coefficients (Fickean or Maxwellean), how they are applied, and the intended use of the resulting model (interpretive or predictive).

The impact of such anomolously high tortuosities ($\tau = 17$) is to produce the concentration polarization described above. However, the apparent success of the predicted current-voltage (I-V) curves is essentially an accident, because SOFC models are sensitive to tortuosity in the high current regime, but insensitive in the lower current regimes where almost any tortuosity will suffice. Tortuosity employed in this manner is essentially an empirical parameter with limited predictive capabilities for developing new SOFC designs. Predictions based on anomolous tortuosities can even be misleading, because such a model may indicate that decreasing the anode thickness or increasing its porosity would be advantageous, at the expense of structural integrity. The mechanisms proposed below for concentration polarization indicate that this may not be the case. The primary purpose of this paper is to develop a model of anodic concentration polarization with more physical meaning, and thus to enable improved predictions.

In the following sections, we first present experimental evidence that supports tortuosities in the range of 2.5-3 for modern SOFC anode materials. This is followed by a description of the proposed mechanisms responsible for concentration polarization: competetive adsorption and surface diffusion near the TPBs. A mathematical model of this scenario is then fitted to experimental fuel cell performance data. The resulting good agreement between fitted model parameters and independent experimental data supports the physical foundations of the model. Conclusions are summarized in the last section.

Experimental Determination of Tortuosities

A classical Wicke-Kallenbach experimental apparatus[8] was assembled and used to determine the tortuosity for porous cermet anode materials in counter diffusion, where the gases diffuse in opposite directions. This is the case in an SOFC anode: the fuels (*e.g.*, H_2 and CO) diffuse toward the anode/electrolyte interface, and the oxidation products (*e.g.*, H_2O and CO_2) diffuse away from that interface. Since an equal number of moles diffuse in each direction, there is no localized gas accumulation to cause internal pressure gradients. Consequently, a near-zero ($<\pm 0.005$ in. H_2O) pressure gradient was maintained across the sample by balancing the flow rates of the gas supplies, thus eliminating Darcian fluxes. Diffusion of gases through the porous anode material was considered to be dominated by bulk gas diffusion and Knudsen diffusion mechanisms. A photomicrograph of the anode material appears on the right side of Fig. 1b, and more detail is given in the section on Fitting the Model to Experimental Data. Data were collected using mass flow controllers and a gas chromatograph, and subsequently analyzed using a

* Electrochemical Society Active Member.
z E-mail: Rick.Williford@pnl.gov

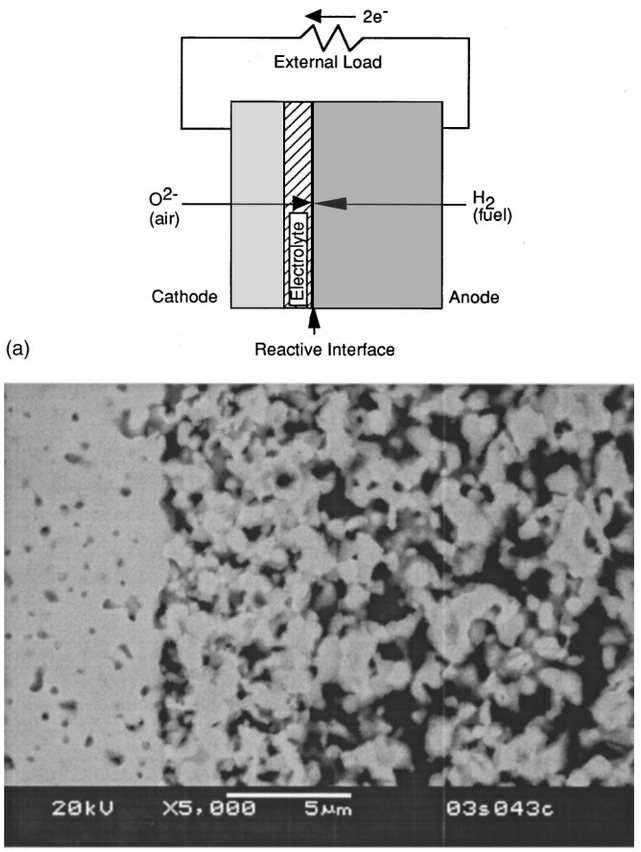

Figure 1. (a) Schematic of an SOFC, showing the reactive zone near the anode/electrolyte interface. (b) Photomicrograph of the anode reactive region. The electrolyte is on the left, and the porous anode is on the right. See text for details.

Maxwell-Stefan formalism to extract the tortuosities. Additional details of the experimental procedure and data analysis methods will be provided in a separate publication.

Tortuosities measured for a range of practical anode porosities are shown in Fig. 3, where they are compared to the results from independent mercury porosimetry experiments. It is evident that modern anode materials with typical porosities (>30%) exhibit tortuosities in the range of 2.5-3.0. In addition, these results are in agreement with work from other laboratories involved with SOFC research,[9,10] where tortuosities of 2.5-6.0 have been experimentally determined, depending on whether or not Knudsen effects have been treated explicitly. (Because bulk gas and Knudsen diffusion are series resistances of comparable magnitude at typical SOFC operating temperatures, failure to properly account for Knudsen effects can result in fitted totuosities that are about a factor of two higher than in Fig. 3.) This is a strong indication that the anomolously high tortuosities mentioned above are artifacts resulting from incomplete models that do not treat all the important phenomena that control SOFC behavior, particularly in the high fuel utilization regimes where concentration polarization can be manifest as a limiting current capacity. The model presented in the next section proposes a solution to this deficiency.

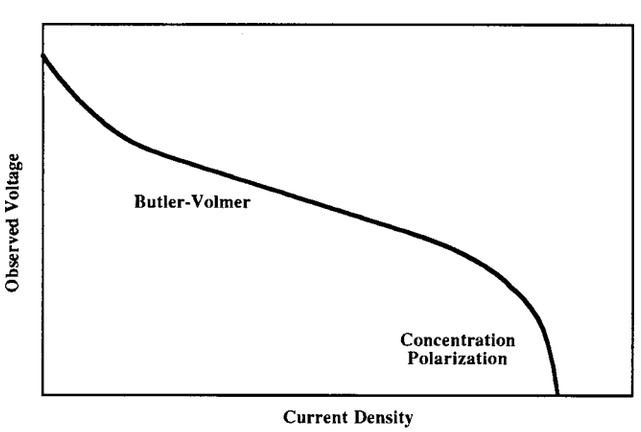

Figure 2. I-V performance of an SOFC, showing the low current Butler-Volmer region and the high current region of anodic concentration polarization.

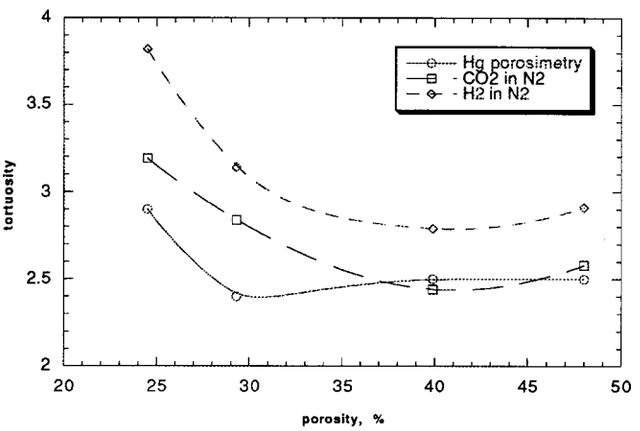

Figure 3. Experimentally determined tortuosities for anode materials.

Possible Sources of Limiting Current Behavior

In the last decade, there have been a substantial number of investigations into SOFC anode behavior with the purpose of identifying the rate-controlling mechanisms under various operating conditions. Many mechanistic theories have been argued, including: reactivities and charge transfer,[11-18] surface diffusion,[13,16,18,19] adsorption,[13,16] sintering and/or impurities,[14,16,20,21] hydrogen desorption rates,[16,22] catalytic effects of water,[22] the role of the YSZ support,[14] and others. Those investigations have employed three types of experimental configurations: porous cermets, pattern anodes, and point contact anodes. Results from such different anode geometries are understandably quite variable. A good graphic demonstration appears in Fig. 3 of Ref. 14, and an excellent review in Ref. 22. In addition to differences in the number of electrochemical impedance spectra (EIS) arcs observed, there are also occasional major differences in conclusions, *e.g.*, which metal (Pt or Ni) appears more reactive.[12,19] Difficulties associated with interpretation of EIS spectra have been recently reviewed,[22-24] and originate in part from the need to assume a specific equivalent circuit model prior to analysis of the data, thus limiting the range of possible conclusions. Finally, the above investigations have apparently not focused specifically on identification of the rate-limiting mechanisms for the condition of high current (or high fuel utilization), which as mentioned above defines the power envelope for the SOFC. This is the subject of the present paper.

The above disparate results in turn lead to differences in the identification of which mechanisms are important or rate-limiting. One important difference between these experimental geometries concerns the supply of reactant gases, and how that supply affects local coverages at the reaction site (see, for example, Ref. 22). For example, a point or pattern electrode in a flowing gas system would not be expected to exhibit significant readsorption of the water vapor created by reaction because that water vapor is removed by the gas

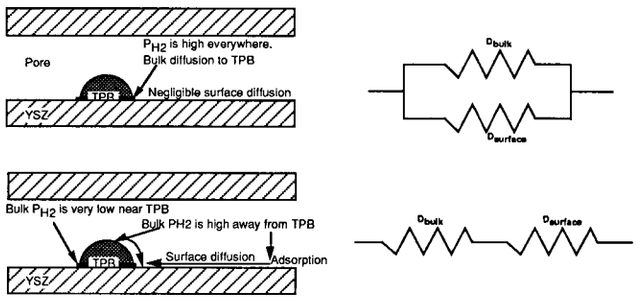

Figure 4. Parallel bulk gas and surface diffusion occurs when reactant partial pressures are high in the TPB region (top diagrams). At low partial pressures caused by high current or high fuel utilization, the diffusion paths operate in series (bottom diagrams).

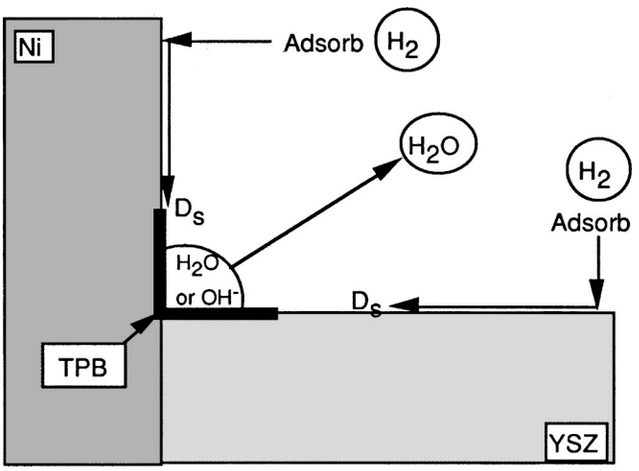

Figure 5. Schematic of the hydrogen circuit in the vicinity of a reactive TPB site. D_s indicates surface diffusion.

stream. This may not be true in a porous cermet, where the water vapor must diffuse out through the pores. Although gas phase H_2-H_2O counter-diffusion effects appear negligible, the presence of more water vapor (and other reaction products) in the immediate vicinity of the reactive TPB site could be expected to reduce the availability of empty surface sites for hydrogen adsorption, surface diffusion, and subsequent reaction. Consequently, competetive adsorption and coverage-dependent surface diffusion would be expected to play a role in cermets, as proposed in the following paragraphs.

At low current, when the demand for reactive TPB sites is low, many reactive sites are unoccupied in the sense that they are available for reactions. Bulk gas and surface diffusion effectively operate in parallel, as in the top diagrams of Fig. 4, to supply reactants to the TPB. Since bulk gas transport and the associated surface collision rate is a much faster process than surface diffusion, the relatively lower flux due to surface diffusion is not important in this case. However, when the current or fuel utilization is high, the demand for reactive sites is also high. Consequently, many reactive sites are occupied by either H or OH waiting for oxidation by an O, or by H_2O waiting to desorb. New reactants cannot reach the TPBs directly from the gas phase, so bulk and surface diffusion operate in series, and the slower surface mechanism controls the supply of reactants to the TPB.

Note that the regions adjacent to the TPBs may exhibit lower reactivity because the majority of the oxygen is drawn to the reactive site at the TPB. These adjacent regions would then be more likely to have surface sites available for reactant adsorption. Because a TPB is essentially an intense reactant sink with associated concentration gradients, the gas atmosphere above the adjacent regions is more likely to be richer in reactants. Both these factors enable adsorption of reactants in the regions adjacent to the TPBs. Transport of the reactants to the TPB reactive sites *per se* must then occur by surface diffusion. In essence, the surfaces adjacent to the TPBs act as ''collectors.'' The reactants adsorbed on the collector regions then diffuse along the surfaces to the TPBs, where they react with oxide ions from the electrolyte to form products. The most effective hydrogen collector is probably the Ni surface, because hydrogen is adsorbed dissociatively there (see, for example, Ref. 24).

When the reactant (hydrogen) reaches a chemically active TPB site (~5 Å wide) occupied by an oxide ion, it reacts due to free energy considerations to form a hydroxyl molecule (~3 Å diam). As more H and O arrive at the reactive site, water molecules form. The reactive site is not large enough to accommodate two water molecules, so one desorbs (or first moves to an adjacent unoccupied surface site and is subsequently desorbed from that location). A diagram of the hydrogen path would thus appear rather circular (see Fig. 5), approaching the TPB along the surface as hydrogen and exiting the TPB through the gas phase as water vapor, thus minimizing intermolecular collisions during diffusion along the surface. This is essentially a ''spillover'' mechanism, as discussed in the literature cited above (see, for example, Ref. 22).

Reactive site occupancy would be consistent with the observation that surface coverage by adsorbed water vapor can be significant even at high temperatures.[25] Surface diffusion of H would control if diffusion times are longer than the residence times of adsorbates. For a 1 μm Ni particle at 800°C, the time for surface diffusion to transport an H atom along the Ni surface to the TPB reaction site is estimated at about 10^{-5} s, whereas the residence time for chemisorbed OH or H_2O on the TPB reaction site is estimated to be a nanosecond or less by classical theory.[16,26] Surface diffusion would therefore appear to be the rate-limiting mechanism.

Mathematical Model for Anode Concentration Polarization

The two primary phenomena that occur to cause concentration polarization at high current in a porous anode are (*i*) competetive adsorption of reactants on less reactive surfaces adjacent to the reactive TPB, and (*ii*) surface diffusion of the reactants from those adjacent surfaces to the reactive TBP site. Competetive adsorption is necessary for two reasons: (*i*) The reactants must reside on a surface to enable reaction with the oxygen ions, which are supplied by solid-state diffusion rather than gas diffusion. (*ii*) Adsorption is competetive because the product gases (H_2O and CO_2) are also present in the gas atmosphere near the TPB, and those gases may also adsorb onto the collection surfaces. Surface diffusion is necessary because the primary adsorption sites are adjacent to the reactive TPB site, and reactants must diffuse along the surface in order to reach the reaction site. Mathematical models for each phenomenon are described below.

As a first approximation, the competetive adsorption isotherms are taken as those given by Langmuir.[26] Monolayer isotherms, rather than multilayer Brunauer-Emmett-Teller isotherms, are employed because the high temperatures result in very low coverages. The surface coverage of species i in a mixed gas is given by

$$\theta_i = \frac{b_i P_i}{1 + \Sigma_i b_i P_i} \qquad [1]$$

where P_i is the species partial pressure over the reactive surface, and b_i is the Langmuir parameter

$$b_i = \frac{N_A A_i \tau_0}{\sqrt{2\pi RTM_i}} e^{Q_i/RT} \qquad [2]$$

N_A is Avogadro's number, A_i is the area of the molecule on the surface (πr^2, where r is the molecular radius), τ_0 is the vibrational period (10^{-13} s), R is the gas constant, T is the absolute temperature, M_i is the species molecular weight, and Q_i is the activation energy for adsorption on the given surface. Note that the partial pressures (P_i) at the reactive interface are determined approximately by the effective bulk diffusion coefficients ($D_{eff(i)} = \phi D_i/\tau$) of the porous medium and a linear Fickean approximation of the flux across the porous anode,[2,3]

$$P_i = P_i^0 - (IRT/2F)l/D_{eff(i)} \quad [3]$$

where P_i^0 is the partial pressure of species i at the anode/gas interface, F is Faraday's constant, I is the current density (A/cm^2), and l is the anode thickness. A minus sign appears before the last term on the right side of this equation for reactants, and a plus sign for products. This approximation is employed by virtue of the null results obtained concerning the presence of nonlinear concentration gradients across the bulk anode.

Because of the high temperatures, surface coverages given by Eq. 1 are very small, whereas the surface diffusion models described below were developed from experimental data generally valid for coverages between 0 and 1. The coverage in Eq. 1 must therefore be scaled so that it applies to the coverage ranges valid for those correlations. For this purpose, the relative coverage (Θ_i), or surface mole fraction, is employed in a manner analogous to the use of the vacancy coverage,[27,28] to reference coverages to the reactive area, rather than to the total surface area

$$\Theta_i = \frac{\theta_i}{\Sigma_i \theta_i} \quad [4]$$

The surface diffusion correlation describes the transition from control by bulk gas diffusion to control by surface diffusion *per se*. The mathematical form for this diffusion transition correlation originated from Vignes[29] in 1966 and was used by Krishna[30,31] and others to address surface diffusion problems in porous media. In the present case, this correlation takes the form

$$D_i^t = D_i^{\Theta_i} D_{s,i}^{1-\Theta_i} \quad [5]$$

where D_i^t is the transition diffusion coefficient, D_i is the gas phase diffusion coefficient, and D_s is the surface diffusion coefficient for species i. D_i is commonly estimated from the average of the binary diffusion coefficients in the mixed gas,[2] weighted by their mole fractions, and does not account for ϕ and τ because the diffusion occurs in the immediate vicinity of the TPB rather than across the porous ceramic. Taking the logarithm of both sides of this equation reveals that it is simply a linear correlation for the exponents of the diffusion coefficients for the controlling mechanisms at high (D_i) and low ($D_{surface}$) surface coverage. Note that the transition correlation is applied only to the burnable fuel gases (H_2 and CO) that must undergo surface diffusion to reach the reactive TPB site. The products H_2O and CO_2 are generated at the TPB, and therefore are in sufficient abundance to contribute only through the competetive adsorption isotherm.

Of the two limiting diffusion coefficients in Eq. 5, the bulk value (D_i) has been discussed above. The other limiting value, the surface diffusion coefficient D_s, must be described in more detail, because it depends on the amount of surface coverage, or the site occupancy. First, note that since the Pacific Northwest National Laboratory (PNNL) SOFC model[2] employs Fickean diffusion concepts and coefficients, D_s must also be expressed in the Fickean formalism for self-consistency, rather than the more rigorous Maxwell-Stefan (MS) formalism. The former deduces essentially empirical diffusion coefficients from overall flux measurements, while the latter seeks coefficients from first principles. In the simplest cases, the two formalisms are related by a thermodynamic coefficient $\Gamma = 1/(1 - \Theta)$ in the equation $D_{Fick} = \Gamma D_{MS}$.

The dependence of D_s on surface coverage has been a subject of debate in the literature, and depends on the range of the coverage as well as whether the coverage is quantified by its absolute (θ_i) or its relative (Θ_i) value. Recent publications have clarified the issue.[28,30] The correlation used here for surface diffusion is the Vignes concept modified by the thermodynamic factor Γ to give the Fickean value

$$D_{s,i} = \frac{D_{s,i,0}^{1-\Theta_i} D_{s,i,1}^{\Theta_i}}{1 - \Theta_i} \quad [6]$$

where $D_{s,i}$ is the Fickean surface diffusion coefficient, Θ_i is the relative coverage of species i, $D_{s,i,0}$ is the surface diffusion coefficient as zero coverage is approached, and $D_{s,i,1}$ is that as full coverage is approached. Such a correlation reproduces the experimentally observed decrease in the generalized MS (GMS) diffusivity with increasing coverage, and the nonmonotonic behavior of the Fickean diffusivity.[28] The Fickean surface diffusivity first decreases with increasing coverage, and then increases sharply as full coverage is approached due to the thermodynamic factor. Note that Eq. 6 again uses the relative coverage rather than the absolute coverage to ensure that the model is properly scaled to experimental results from the literature. Also note that $D_{s,i,0}$ at low coverage is expected to be much larger than $D_{s,i,1}$ at high coverage because fewer surface sites are occupied, so the jump distance or jump frequency is larger at low coverage. These general trends are observed in the next section, where the model is fit to experimental data.

Fitting the Model to Experimental Data

A series of experiments were conducted in our laboratory using anode-supported single cell SOFCs. The "button cell" sample configurations for these experiments were prepared as follows. Anode/electrolyte (NiO-YSZ/YSZ) substrate samples were produced via standard organic tape-casting and tape lamination procedures, cosintered at 1375°C for 1 h, and subsequently creep-flattened at 1350°C for 2 h. The postsintered/postreduced anode (~500 μm thick) was comprised of a bulk layer with a solids ratio of 40/60 vol % Ni/YSZ (and approximately 30 vol% porosity), and a 5-10 μm thick active anode layer with 50/50 solids vol % Ni/YSZ (see Fig. 1b). The sintered thickness of the YSZ electrolyte membrane was 5-10 μm thick. A $Ce_{0.8}Sm_{0.2}O_{1.9}$ (SDC-20) interlayer (~5 μm postsintered thickness) was applied to creep-flattened anode substrates via screen printing, and sintered at 1200°C for 2 h. The cathode ($La_{0.8}Sr_{0.2}FeO_{3-\delta}$-LSF-20) was also applied by screen printing and sintered at 1150°C for 2 h (25-40 μm postsintered thickness). The diameter of the anode support was 2.5 cm, and that of the screen-printed cathode initially 2.2 cm. The cathode area (3.8 cm^2) was used as the active cell area to calculate current and power densities. Screen-printed Pt grids with embedded Pt gauze, and screen-printed NiO grids with embedded Ni gauze were used as current collectors for the cathode and anode, respectively. The cells were sealed to alumina test fixtures using Aremco cements, and I-V data recorded at 750°C using an Arbin BT2000 potentiostat-galvanostat electrochemical testing system; cells were held at 0.7 V and periodically subjected to current sweeps from 0-7 A. Fuel was flowed to the anode at 200 standard cubic centimeters per minute (sccm), and air to the cathode at 300 sccm. I-V performance curves (Fig. 6) were generated for a range of fuel compositions varying from 9.7 to 97% H_2, with 3% water vapor, the balance being N_2. Additional details of these experiments have been reported in another publication.[32] The above described model for anode concentration polarization was benchmarked to data collected from these experiments, as described in the following paragraphs.

To reproduce the precipitous voltage drops at the limiting currents shown in Fig. 6, three parameters must be fit: the activation energy (Q_{H2}) for hydrogen adsorption in Eq. 2, and the low-coverage

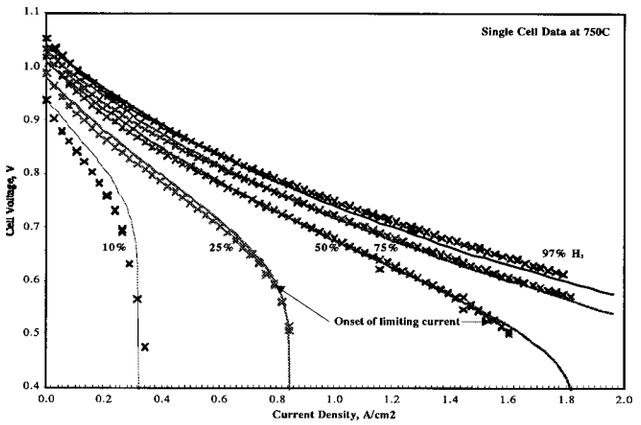

Figure 6. Comparison of the model (solid curves) to the experimental data (symbols). Numbers show the percent H_2 in the fuel stream. All data were taken at 750°C.

($D_{s,H2,0}$) and high coverage ($D_{s,H2,1}$) surface diffusivities in Eq. 6. As a first approximation, the adsorption activation energies for the other gases were taken as 0.5 eV/molecule. Since hydrogen was the only combustible gas in the test fuel, it was the only gas for which the above surface diffusivities were sought. The PNNL SOFC electrochemical model,[2] supplemented by the above anode concentration polarization model, was used for fitting in a standard multivariable least squares routine.[33] The best results for an assumed tortuosity of 2.5 (see Fig. 3) were found for the following combination of parameters: $Q_{H2} = 0.425$ eV/molecule, $D_{s,H2,0} = 0.10805$ cm^2/s, and $D_{s,H2,1} = 5.64088 \times 10^{-4}$ cm^2/s. Comparison of these parameters to experimental data from independent sources is discussed below.

Because hydrogen adsorbs dissociatively on Ni,[34,35] it was assumed that the supply of hydrogen atoms for the reaction was dominated by this surface, rather than the YSZ.[24] The adsorption energy found above ($Q_{H2} = 0.425$ eV/molecule at 1023 K) is in good agreement with quantum mechanics calculations[34] (0.2-0.4 eV/molecule, depending on the crystal face) for dissociative adsorption of H_2 on Ni surfaces. It is understandably less than the apparent energies often interpreted from EIS spectra ($\sim$1 eV/molecule), because those values can include other activated processes, such as surface diffusion, that cannot be extracted unambiguously from the EIS spectra (see, for example, Ref. 13).

The hydrogen surface diffusion coefficients also appear reasonable when compared to other data. At very low relative coverage and high temperatures, D_s may approach the bulk gas value due to the high availability of vacant surface sites for diffusion by atomic hopping mechanisms. This permits either large hopping distances or high hopping rates. The value of $D_{s,H2,0} = \sim 0.1$ cm^2/s seems reasonable compared to the bulk gas value of about 7 cm^2/s. At higher surface coverages, D_s is expected to be greatly reduced from its low coverage value due to higher occupation of surface sites by the various gases in the mixture. The fitted value of $D_{s,H2,1} = 5.64 \times 10^{-4}$ cm^2/s is in good agreement with experimental data for hydrogen on Ni (4.8-6.8 $\times 10^{-4}$ cm^2/s) from an extensive review by Seebauer and Allen.[36]

Last, the result $D_{s,H2,0} \gg D_{s,H2,1}$ is consistent with expectation based on experimental observation[37] and kinetics arguments (see Ref. 28, Eq. 27-29, and Ref. 30, Eq. 35-38). Consequently, the model parameters derived from the fitting exercise are in good agreement with independent data, indicating that the physical foundations of the model are credible.

Discussion

To put the model in the proper perspective, it is useful to realize some of its more important limitations, as follows. The data base for fitting the parameters of this model is rather limited, and the model has not been tested on other well-characterized experimental data sets. Consequently, the model must be considered as preliminary or approximate until further experimental data become available. Although simulations over a temperature range of 650 to 800°C gave good agreement with experiment, additional data using mixed gas fuels (H_2, CO, CO_2, H_2O, and N_2) will be needed to refine the activation energies (Q) and surface diffusion coefficients (D_s) for those gases. Also, the effects of the cathode have not been separated out in the data. Although cathodic limitations are expected to be minimal in these experiments, this should be checked using, *e.g.*, impedance spectroscopy techniques.

Several aspects of the adsorption models could be refined. The basic Langmuir isotherm was assumed as a starting model, and should be confirmed experimentally using actual SOFC materials. Although Ni is thought to play the dominant role in providing hydrogen atoms for reaction at the TPB via dissociative adsorption,[16,38] questions remain concerning the roles of its surface crystallography, roughness and oxidation state, and how they affect the adsorption energy.[22,34] The role of impurities and variations in manufacturing methods on the adsorption/desorption behavior for OH and H_2O on the Ni and YSZ surfaces are not well understood, and are thought to introduce appreciable scatter.[14,16,39,40]

Positive attributes of the present model include the following. Although the reaction is limited to the TPB site, the adsorption and diffusional roles of the adjacent Ni and YSZ areas are incorporated. Thus, the model contains a simplified version of the modern catalytic spillover phenomena discussed in the literature (see, for example, Ref. 22). Apparent activation energies derived from EIS data range between 0.8 and 1.3 eV for cermet anodes.[14] The present analysis gave 0.425 eV for the hydrogen dissociative adsorption process, which seems reasonable since it would be expected to be only a portion of an overall apparent activation process.

One of the most important problems is the identification of rate-limiting processes for SOFC electrochemical systems. Interpretation of EIS data alone is apparently insufficient for definitive identification (see, for example, Ref. 23). One of the main problems is that an equivalent circuit model must be assumed before the analysis can proceed, and this in a sense predetermines many of the possible conclusions that can be reached. However, a noteworthy recent trend is the introduction of molecular-scale kinetics into the spectral models.[24] This is an advancement over simply assuming an adsorption isotherm. It increases interpretive power, but at the expense of increased data requirements for kinetic coefficients. In time, this data deficiency will be alleviated. Meanwhile, it may be useful to solve smaller portions of the problem, such as the focus on concentration polarization in the present paper. This can be viewed, for example, in the context of the proposed catalytic effect of water vapor.[22] If water provides a catalytic enhancement at low overpotentials (*i.e.*, in the concentration polarization region), then some another mechanism must be active to limit the current output. We propose that this mechanism is a combination of competetive adsorption and surface diffusion, coupled as described by the dependence of the surface diffusion coefficient on the coverage (Eq. 5 and 6). Although this does not rule out the possible roles of of other limiting mechanisms, such as oxide ion diffusion through the YSZ,[14,22] at least the number of such mechanisms appears to be reduced compared to those encountered when addressing the entire range of SOFC performance in a single model.

Even supported only by the above-limited evidence, the potential impacts of the proposed model should be realized. An important result is that the diffusional resistance of modern porous ceramic anode materials is not in the bulk of the material, but rather is localized near the electrode/electrolyte interface, where the oxidation reaction occurs. Models incorporating such concepts can accelerate SOFC development by providing improved predictions of lim-

iting current behavior, thus better defining SOFC performance envelopes. Such models can also provide guidance concerning research topics for SOFC improvements: the appropriate focus should not be on anode bulk porosity or anode thickness, but rather on optimization of localized reactivitiy, competetive adsorption, and surface diffusion at the electrode/electrolyte interface.

Conclusions

Experimental evidence from several laboratories has indicated that the tortuosities of modern porous ceramic SOFC anode materials are not as high as previously invoked ($\tau = 17$). The diffusional resistance of anodes therefore cannot be a bulk effect, but rather is localized at the anode/electrolyte interface. At high currents (high fuel utilizations), the two primary phenomena responsible for this interface diffusional resistance appear to be (i) the competetive adsorption of fuel gases on less reactive sites near the TPBs, followed by (ii) surface diffusion to the reactive sites at the TPBs. Fitting of the adsorption energy and surface diffusion coefficients to a well-characterized SOFC performance data set produced good agreement with independent experimental data for H_2, indicating that the proposed model is physically reasonable and at least possible. Further experiments on a range of SOFC fuel gases of interest are needed to show that the model is indeed probable. Such experiments should focus on the electrode/electrolyte interface in an effort to optimize the reactive area, adsorption, and surface diffusion mechanisms responsible for the localized diffusional resistance that produces the observed concentration polarization at high fuel utilization.

Acknowledgments

This work was supported by the Solid-State Energy Conversion Alliance (SECA), the National Energy Technology Laboratory, the Office of Fossil Energy, and the U.S. Department of Energy. Pacific Northwest National Laboratory is operated for the U.S. Department of Energy by Battelle Memorial Institute.

PNNL assisted in meeting the publication costs of this article.

List of Symbols

A_i	area of molecule of species i on a surface
b_i	Langmuir coefficient for species i
D_i	diffusion coefficient for species i in the bulk gas phase
$D_{eff(i)}$	effective gas phase diffusion coefficient for species i
D_i^t	transition diffusion coefficient for species i
$D_{s,i}$	surface diffusion coefficient for species i
$D_{s,i,0}$	surface diffusion coefficient at low coverage
$D_{s,i,1}$	surface diffusion coefficient at high coverage
F	Faraday's constant
M_i	molecular weight of species i
N_A	Avogadro's number
P_i	partial pressure of species i at the TPB
P_i^0	partial pressure of species i at the anode/gas surface
Q_i	adsorption activation energy for species i
R	gas constant
T	absolute temperature
TPB	phase boundary
YSZ	yttrium stabilized zirconia

Greek

Γ	thermodynamic coefficient
Θ_i	relative coverage of species i
θ_i	absolute coverage of species i
ϕ	porosity
τ	tortuosity
τ_0	vibrational period

References

1. N. Q. Minh and T. Takahashi, *Science and Technology of Ceramic Fuel Cells*, Elsevier Publishers, Amsterdam (1995).
2. L. A. Chick, J. W. Stevenson, K. D. Meinhardt, S. P. Simner, J. E. Jaffe, and R. E. Williford, *Modeling and Performance of Anode Supported SOFC, Fuel Cell Seminar Abstracts*, Courtesy Associates, p. 619 (2002).
3. J. W. Kim, A. V. Virkar, K. Z. Fung, K. Mehta, and S. C. Singhal, *J. Electrochem. Soc.*, **146**, 69 (1999).
4. P. Costamagna and K. Honegger, *J. Electrochem. Soc.*, **145**, 3995 (1998).
5. C. N. Satterfield and P. J. Cadle, *Ind. Eng. Chem. Fundam.*, **7**, 202 (1968).
6. S. K. Bhatia, *AIChE J.*, **34**, 1094 (1988).
7. R. Krishna and J. A. Wesslingh, *Chem. Eng. Sci.*, **52**, 861 (1997).
8. J. Haugaard and H. Livberg, *Chem. Eng. Sci.*, **53**, 2941 (1998).
9. I. Drescher, W. Lehnert, and J. Meusinger, *Electrochim. Acta*, **43**, 3059 (1998).
10. W. Lehnert, J. Meusinger, and F. Thom, *J. Power Sources*, **87**, 57 (2000).
11. J. Mizusaki, H. Takagawa, K. Isobe, M. Tajika, I. Koshiro, H. Maruyama, and K. Hirano, *J. Electrochem. Soc.*, **141**, 1674 (1994).
12. D. Kek, N. Bonanos, M. Mogensen, and S. Pejovnik, *Solid State Ionics*, **131**, 249 (2000).
13. S. P. Jiang and S. P. S. Badwal, *Solid State Ionics*, **123**, 209 (1999).
14. M. Brown, S. Primdahl, and M. Mogensen, *J. Electrochem. Soc.*, **147**, 475 (2000).
15. B. de Boer, M. Gonzales, H. J. M. Bouwmeester, and H. Verweij, *Solid State Ionics*, **127**, 269 (2000).
16. M. Mogensen and S. Skaarup, *Solid State Ionics*, **86-88**, 1151 (1996).
17. P. Holtappels, L. G. J. de Haart, and U. Stimming, *J. Electrochem. Soc.*, **146**, 1620 (1999).
18. P. Holtappels, I. C. Vinke, L. G. J. de Haart, and U. Stimming, *J. Electrochem. Soc.*, **146**, 2976 (1999).
19. J. Mizusaki, H. Takagawa, T. Saito, K. Kamitani, T. Yamamura, K. Hirano, S. Ehara, T. Takagi, T. Hikita, M. Ippommatsu, S. Hakagawa, and K. Hashimoto, *J. Electrochem. Soc.*, **141**, 2129 (1994).
20. K. V. Jensen, S. Primdahl, I. Chorkendorff, and M. Mogensen, *Solid State Ionics*, **144**, 197 (2001).
21. H. Itoh, T. Yamamoto, M. Mori, T. Horita, N. Sakai, H. Yokokawa, and M. Dokiya, *J. Electrochem. Soc.*, **144**, 641 (1997).
22. B. Bieberle, L. P. Meier, and L. J. Gauckler, *J. Electrochem. Soc.*, **148**, A646 (2001).
23. B. Bieberle and L. J. Gauckler, *Solid State Ionics*, **135**, 337 (2000).
24. B. Bieberle and L. J. Gauckler, *Solid State Ionics*, **146**, 23 (2002).
25. S. Raz, K. Sasaki, J. Maier, and I. Reiss, *Solid State Ionics*, **143**, 181 (2000).
26. A. W. Adamson, *Physical Chemistry of Surfaces*, p. 450, Interscience Publishers, New York (1960).
27. M. Ihara, T. Kusano, and C. Yokoyama, *J. Electrochem. Soc.*, **148**, A209 (2001).
28. R. Krishna, *Chem. Eng. Sci.*, **45**, 1779 (1990).
29. A. Vignes, *Ind. Eng. Chem. Fundam.*, **5**, 189 (1966).
30. R. Krishna, *Chem. Eng. Sci.*, **48**, 845 (1993).
31. R. Krishna, *Chem. Eng. Sci.*, **52**, 861 (1997).
32. S. P. Simner, *Electrochem. Solid-State Lett.*, **5**, A173 (2002).
33. W. H. Press, B. P. Flannery, S. A. Teukolsky, and W. T. Vettering, *Numerical Recipes*, Chap. 14, Cambridge University Press, New York (1986).
34. T. N. Truong, D. G. Truhlar, and B. C. Garrett, *J. Phys. Chem.*, **93**, 8227 (1989).
35. A. V. Hamza and R. J. Madix, *J. Phys. Chem.*, **89**, 5381 (1985).
36. E. G. Seebauer and C. E. Allen, *Prog. Surf. Sci.*, **49**, 256 (1995).
37. C. G. Pope, *Trans. Faraday Soc.*, **63**, 734 (1967).
38. K. Christmann, *Surf. Sci. Rep.*, **9**, 1 (1988).
39. M. Mogensen, K. V. Jensen, M. J. Jorgensen, and S. Primdahl, *Solid State Ionics*, **150**, 123 (2002).
40. M. A. Henderson, *Surf. Sci. Rep.*, **46**, 1 (2002).